

Simultaneous observation of small- and large-energy-transfer electron-electron scattering in three dimensional indium oxide thick films

Yang Yang, Xin-Dian Liu, and Zhi-Qing Li*

Tianjin Key Laboratory of Low Dimensional Materials Physics and Preparing Technology,
Department of Physics, Tianjin University, Tianjin 300072, China

(Dated: June 16, 2021)

In three dimensional (3D) disordered metals, the electron-phonon (*e-ph*) scattering is the sole significant inelastic process. Thus the theoretical predication concerning the electron-electron (*e-e*) scattering rate $1/\tau_\varphi$ as a function of temperature T in 3D disordered metal has not been fully tested thus far, though it was proposed 40 years ago [A. Schmid, Z. Phys. **271**, 251 (1974)]. We report here the simultaneous observation of small- and large-energy-transfer *e-e* scattering in 3D indium oxide thick films. In temperature region of $T \gtrsim 100$ K, the temperature dependence of resistivities curves of the films obey Bloch-Grüneisen law, indicating the films possess degenerate semiconductor characteristics in electrical transport property. In the low temperature regime, $1/\tau_\varphi$ as a function of T for each film can not be ascribed to *e-ph* scattering. To quantitatively describe the temperature behavior of $1/\tau_\varphi$, both the 3D small- and large-energy-transfer *e-e* scattering processes should be considered (The small- and large-energy-transfer *e-e* scattering rates are proportional to $T^{3/2}$ and T^2 , respectively). In addition, the experimental prefactors of $T^{3/2}$ and T^2 are proportional to $k_F^{-5/2}\ell^{-3/2}$ and E_F^{-1} (k_F is the Fermi wave number, ℓ is the electron elastic mean free path, and E_F is the Fermi energy), respectively, which are completely consistent with the theoretical predications. Our experimental results fully demonstrate the validity of theoretical predications concerning both small- and large-energy-transfer *e-e* scattering rates.

PACS numbers: 73.23.-b, 73.20.Fz, 72.15.Qm

I. INTRODUCTION

Four decades ago, the inelastic scattering of the electrons of an impure metal by a screened Coulomb interaction had been investigated.¹ It had been found that the electron-electron (*e-e*) scattering rate $1/\tau_{ee}$ in three dimensional (3D) disordered metal can be expressed as,¹⁻³

$$\frac{1}{\tau_{ee}} = \frac{\pi}{8} \frac{(k_B T)^2}{\hbar E_F} + \frac{\sqrt{3}}{2\hbar\sqrt{E_F}} \left(\frac{k_B T}{k_F \ell} \right)^{3/2}, \quad (1)$$

where E_F is Fermi energy, k_F is the Fermi wave number, ℓ is the mean free path of electrons, T is the temperature, k_B is the Boltzmann constant and \hbar is the Planck constant divided by 2π . The first and second terms on the right hand side of Eq. (1) represent the large- and small-energy-transfer *e-e* scattering processes and dominate at energy scale $\varepsilon > \hbar/\tau_e$ and $\varepsilon < \hbar/\tau_e$, respectively, where τ_e is the electron elastic mean free time.^{2,3} However, the validity of Eq. (1) has not been completely tested⁴⁻⁸ due to the *e-e* scattering is negligible compared with electron-phonon (*e-ph*) scattering in general 3D disordered metals.⁹⁻¹¹ Taking advantage of the low concentration and free-electron-like electrical transport properties of charge carrier in Sn doped In_2O_3 (ITO),^{12,13} Zhang *et al* recently tested the correctness of the small-energy-transfer term in Eq. (1) in ITO thick films.¹⁴ In the present paper, we fully demonstrate the validity of Eq. (1) (including both large- and small-energy-transfer terms) in In_2O_3 thick films. Our results concerning the electrical transport properties and dephasing mechanism of this low carrier concentration and large $k_F \ell$ material are presented and discussed below.

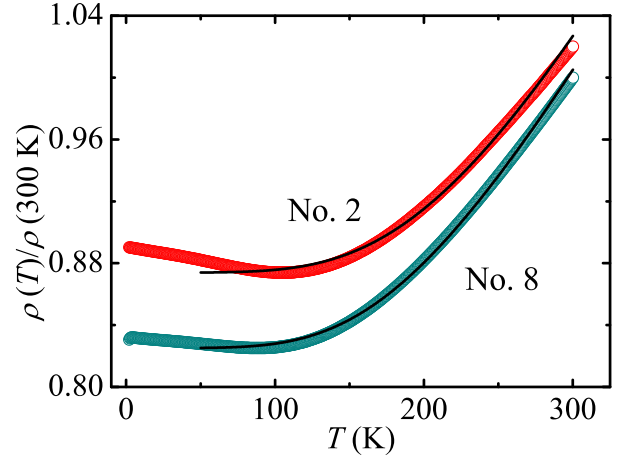


FIG. 1. (Color online) Normalized resistivity as a function of temperature for films Nos. 2 and 8, films. The solid curves are least-squares fits to Eq. (2). For clarify, the data for film No. 2 has been shifted by +0.02.

II. EXPERIMENTAL METHODS

In_2O_3 films were deposited on the (100) yttrium stabilized ZrO_2 (YSZ) single crystal substrates by standard rf-sputtering method. An In_2O_3 target with purity of 99.99% and diameter of 60 mm was used as the sputtering source. The base pressure of chamber was less than 1×10^{-4} Pa, and the sputtering was carried out in argon atmosphere with pressure of 0.55 Pa. In the

depositing process, the substrate temperature was kept at 703, 723, 743, 763, 803, 823, 843, and 923 K, respectively, to tune the charge concentration and the disorder degree of the film. Hall-bar-shaped samples (1-mm wide and 3.6-mm long), deposited by using metal masks,^{14,15} were used to measure the electrical transport properties. The thicknesses of the films ranging from ~ 950 nm to ~ 1100 nm were measured using a surface profiler (Dektak, 6M). The structures of the films were determined by x-ray diffraction (XRD) with $\text{CuK}\alpha$ radiation. The measurements include normal θ - 2θ , ϕ , and ω scans. The XRD results indicate that the films are epitaxially grown on (100) YSZ substrates along [100] direction. The Hall coefficient, longitudinal resistivity and low-field magnetoconductivity were measured on a physical property measurement system (PPMS-6000, Quantum Design) by four-probe method. In the magnetoconductivity measurements, the magnetic field was applied perpendicular to the film plane.

III. RESULTS AND DISCUSSION

Figure 1 shows the resistivity ρ as a function of temperature T for two representative In_2O_3 films, as indicated. The resistivities decrease with decreasing temperatures from 300 to ~ 100 K, reach their minimum and then increase with further decreasing temperature down to our minimum measuring temperature, 2 K. We compare the $\rho(T)$ data at higher temperature region with Bloch-Grüneisen law¹⁶

$$\rho = \rho_0 + \beta T \left(\frac{T}{\theta_D} \right)^4 \int_0^{\theta_D/T} \frac{x^5 dx}{(e^x - 1)(1 - e^{-x})}, \quad (2)$$

where ρ_0 is the residual resistivity, β is a constant, θ_D is the Debye temperature. The solid curves in Fig. 1 are least-squares fits to Eq. (2). The resistivity data can be well described by Eq. (2), indicating In_2O_3 films possess highly degenerate semiconductor characteristic in electrical transport properties. The fitted values of θ_D are listed in Table I. Similar to Sn doped In_2O_3 ¹² and F doped SnO_2 ,¹⁷ our In_2O_3 films also possess higher Debye temperature. The enhancement in resistivity with decreasing temperature below ~ 100 K can be attributed to the weak-localization (WL) and electron-electron interaction effects,^{18–22} which is similar to that in ITO^{8,12} and FTO.¹⁷ The temperature behavior of resistivity of the In_2O_3 films in higher temperature regime indicate In_2O_3 possesses degenerate semiconductor characteristic in transport properties. In fact, the origins of the high conductivity and degenerate semiconductor characteristic of In_2O_3 are still enigmatic. The oxygen vacancy is generally considered as the main contribution to the high conductivity of the undoped In_2O_3 .^{23–30} However, recent theoretical results indicate that the donor level of oxygen vacancies is too deep to produce large densities of free electrons at room temperature.³¹ The reasons that In_2O_3 possesses relative high carrier concentration and

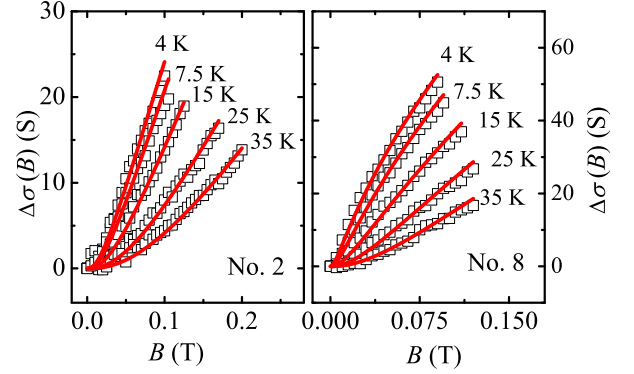


FIG. 2. (Color online) Magnetoconductivity versus magnetic field for films Nos. 2 and 8 measured at different temperatures. The magnetic field was applied perpendicular to the film plane. The solid curves are least-squares fits to Eq. (3).

behaves as degenerate semiconductor in electrical transport properties deserve further investigations.

Figure 2 shows the magnetoconductivity, $\Delta\sigma = \sigma(B) - \sigma(0)$, as a function of magnetic field at low temperatures (4–35 K) for two representative films, as indicated. We found that the magnetoconductivity is positive and its magnitude at a certain field decrease with increasing temperature. These features indicate that the spin-orbit scattering is weak, and the WL effect governs the behaviors of $\sigma(B)$ at low field region.^{9,21,22} Considering the thicknesses of all samples are $\sim 1 \mu\text{m}$, we analyse the magnetoconductivity data using 3D WL theory. In 3D disordered conductors, the magnetoconductivity due to WL effect is given by^{32–36}

$$\Delta\sigma = \sigma(B) - \sigma(0) = \frac{e^2}{2\pi^2\hbar} \sqrt{\frac{eB}{\hbar}} f_3 \left(\frac{B}{B_\varphi} \right), \quad (3)$$

where e is the elementary charge, D is the diffusion constant, and $B_\varphi = B_0 + B_i$. The characteristic field B_j is defined by $B_j = \hbar/(4eD\tau_j)$, where $j = 0$ and i represent the T -independent and inelastic scattering fields (τ_j is the corresponding relaxation time), respectively. The theoretical predictions of Eq. (3) are least squares fitted to our magnetoconductivity data and are shown as solid curves in Fig. 2. Our magnetoconductivity data can be well described by Eq. (3). For the samples, the obtained electron dephasing length $L_\varphi = \sqrt{D\tau_\varphi} = \sqrt{\hbar/(4eB_\varphi)}$ at 4 K varies from ~ 90 to ~ 380 nm, which much less than the thicknesses of the films. Hence our films are 3D with regard to WL effect.

Figure 3 shows the extracted electron dephasing rate as a function of T for the two representative films, as indicated. As mentioned above, the e -ph scattering is the dominant electron dephasing mechanism in 3D general disordered metals.^{9–11} Assuming the e -ph scattering mechanism governs the electron dephasing processes of the films, we quantitatively analyze the $1/\tau_\varphi(T)$ data now. Theoretically, the electron scattering by transverse

TABLE I. Sample parameters for the eight 3D In₂O₃ films. T_s is the substrate temperature during deposition, d is the mean film thickness, ρ is the resistivity, n is the carrier concentration, and θ_D is the Debye temperature. $1/\tau_0$, A_{ee}^S , and A_{ee}^L are defined in Eq. (1). $(A_{ee}^S)^{th}$ and $(A_{ee}^L)^{th}$ are the theoretical values of A_{ee}^S , and A_{ee}^L predicted by Eq. (1).

Film	T_s (K)	d (nm)	$\rho(300\text{ K})$ (m Ω cm)	θ_D (K)	$k_F l$	$n(10\text{ K})$ (10^{19} cm^{-3})	$1/\tau_\varphi^0$ (10^{-9} s^{-1})	A_{ee}^S ($\text{K}^{-3/2}\text{ s}^{-1}$)	A_{ee}^L ($\text{K}^{-2}\text{ s}^{-1}$)	$(A_{ee}^S)^{th}$ ($\text{K}^{-3/2}\text{ s}^{-1}$)	$(A_{ee}^L)^{th}$ ($\text{K}^{-2}\text{ s}^{-1}$)
1	703	1093.60	1.52	1456	8.9	3.83	0.88	1.28×10^8	3.02×10^7	1.23×10^8	4.27×10^7
2	723	1068.36	2.50	1399	5.3	4.06	14.2	1.69×10^8	2.81×10^7	2.64×10^8	4.11×10^7
3	743	1050.98	2.55	1399	5.1	3.91	1.74	1.61×10^8	2.67×10^7	2.79×10^8	4.21×10^7
4	763	1067.45	2.37	1373	5.6	4.26	23.9	1.52×10^8	2.54×10^7	2.38×10^8	3.97×10^7
5	803	1033.56	1.89	1365	6.7	4.92	16.6	1.37×10^8	2.43×10^7	1.72×10^8	3.61×10^7
6	823	1002.18	1.67	1313	7.9	4.71	20.9	1.20×10^8	2.32×10^7	1.37×10^8	3.72×10^7
7	843	1016.62	1.50	1335	8.5	5.22	1.84	1.20×10^8	2.24×10^7	1.20×10^8	3.47×10^7
8	923	952.93	1.31	1236	9.1	6.31	2.43	1.15×10^8	1.87×10^7	1.01×10^8	3.06×10^7

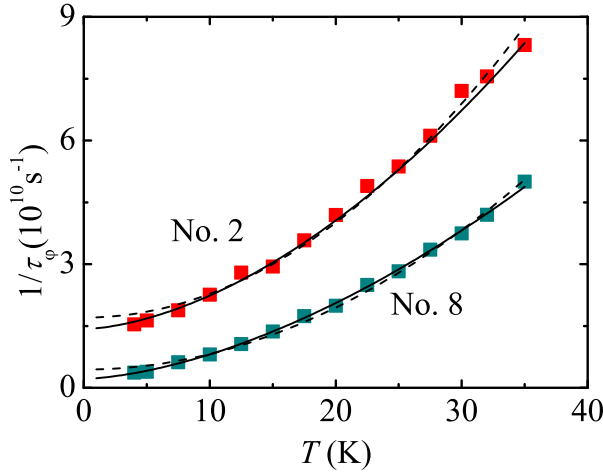


FIG. 3. (Color online) The electron dephasing rate as a function of temperature for films Nos. 2 and 8. The dash curves are least-squares fits to Eq. (5), and the solid curves are least-squares fits to Eq. (6).

vibrations of defects and impurities dominates the e -ph relaxation. In the quasiballistic limit of $q_T \ell > 1$ (where q_T is the wave number of a thermal phonon), the relaxation rate, $1/\tau_{e-t,\text{ph}}$, is given by^{37,38}

$$\frac{1}{\tau_{e-t,\text{ph}}} = \frac{3\pi^2 k_B^2 \beta_t T^2}{(p_F u_t)(p_F \ell)}, \quad (4)$$

where $\beta_t = (2E_F/3)^2 N(E_F)/(2\rho_m u_t^2)$ is the electron-transverse phonon coupling constant, p_F is the Fermi momentum, u_t is the transverse sound velocity, ρ_m is the mass density, and $N(E_F)$ is the electronic density of states at the Fermi level. For our films, the values of $q_T \ell$ vary from $\sim 0.3T$ to $\sim 0.5T$.³⁹, which are greater than unity for $T \geq 4\text{ K}$. Our $1/\tau_\varphi(T)$ data from 4 to 35 K were least-squares fitted to the following equation:

$$\frac{1}{\tau} = \frac{1}{\tau_0} + \tilde{A}T^2, \quad (5)$$

where $1/\tau_0$ stands for the saturated dephasing rate,^{40–42} and \tilde{A} is an adjustable parameter and presumably represents the e -ph scattering strength given in Eq. (4). The dash curves in Fig. 3 are the fitted results. Clearly, the experimental dephasing rate can be described by the T^2 term at high temperature regime ($T \gtrsim 10\text{ K}$), while it deviate from the predication of Eq. (5) for $T < 10\text{ K}$. The fitted values of \tilde{A} vary from $\sim 3.8 \times 10^7$ to $\sim 5.8 \times 10^7\text{ K}^{-2}\text{ s}^{-1}$. On the other hand, the values of u_t and ρ_m of In₂O₃ are 2400 ms^{-1} and 7100 kg m^{-3} ,⁴³ respectively, the carrier concentrations vary from 3.8×10^{19} to $6.3 \times 10^{19}\text{ cm}^{-3}$, and the effective mass of electron m^* can be taken as $m^* = 0.4m_e$,⁴⁴ where m_e is the free-electron mass. According to Eq. (4), one can readily obtain that the theoretical values of e -ph scattering strength $A_{e-t,\text{ph}}$ [the prefactor of T^2 in Eq. (4)] vary between $\sim 1.2 \times 10^5$ to $\sim 2.2 \times 10^5\text{ K}^{-2}\text{ s}^{-1}$, which are two orders of magnitudes less than the values of \tilde{A} . Thus the e -ph scattering rate is negligibly weak in our 3D In₂O₃ films.

In the framework of free-electron model, one can deduce the e -ph relaxation rate $1/\tau_{e-t,\text{ph}} \propto n$ from Eq. (4), where n is the carrier concentration. However, Eq. (1) predicates $1/\tau_{ee}^L \propto n^{-2/3}$ and $1/\tau_{ee}^S \propto n^{-4/3}$, where τ_{ee}^L and τ_{ee}^S represent the large- and small-energy-transfer e - e relaxation time, respectively. For the In₂O₃ films, the carrier concentration is around $\sim 5 \times 10^{19}\text{ cm}^{-3}$, which is ~ 3 to ~ 4 orders of magnitudes less than that of typical metals. Hence the e - e scattering rate could be much greater than the e -ph scattering rate in this low carrier concentration compound. The $1/\tau_\varphi(T)$ data were then least-squares fitted to the following equation:

$$\frac{1}{\tau} = \frac{1}{\tau_0} + A_{ee}^S T^{3/2} + A_{ee}^L T^2, \quad (6)$$

where the second and third terms on the right-hand side of Eq. (6) stand for the small- and large-energy-transfer e - e scattering terms, respectively. The solid curves in Fig. 3 are the theoretical predication of Eq. (6). Inspection of Fig. 3 indicates that the experimental dephasing rate can

be well described by Eq. (6) in the whole measuring temperature range. The obtained values of A_{ee}^S and A_{ee}^L , as well as $1/\tau_\varphi^0$, are listed in Table I. Using free-electron-like model, one can easily obtain the theoretical values of A_{ee}^S and A_{ee}^L [see Eq. (1)], denoted as $(A_{ee}^S)^{\text{th}}$ and $(A_{ee}^L)^{\text{th}}$ and also listed in Table I, respectively. For most of the films, the values of A_{ee}^S are nearly equal to the theoretical ones, except for films Nos. 2, 3 and 4. Even for the three films, the values of A_{ee}^S and $(A_{ee}^S)^{\text{th}}$ agree to within a factor of ~ 2 or smaller. Also, our experimental values of A_{ee}^L are within a factor of ~ 1.6 of $(A_{ee}^L)^{\text{th}}$. These levels of agreement are satisfactory. Thus, both the small- and large-energy-transfer e - e scattering processes govern the dephasing in these 3D In_2O_3 films. Inspection the experimental values of A_{ee}^S and A_{ee}^L indicates that the large-energy-transfer e - e dephasing rate is about one-half of that of the small-energy-transfer one even at 5 K for each film.

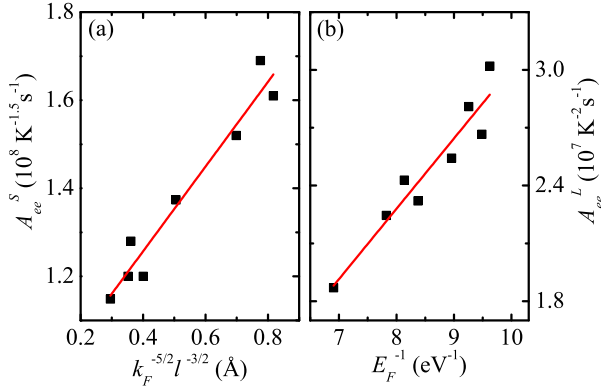


FIG. 4. (Color online) (a) The small-energy-transfer e - e scattering strength A_{ee}^S as a function of $k_F^{-5/2}\ell^{-3/2}$. (b) The large-energy-transfer e - e scattering strength A_{ee}^L as a function of E_F^{-1} . The solid lines are the linear fits to the experimental data.

According to Eq. (1), the parameters A_{ee}^S and A_{ee}^L in Eq. (6) should obey $A_{ee}^S \propto E_F^{-1/2}(k_F\ell)^{-3/2}$ and $A_{ee}^L \propto E_F^{-1}$, respectively. (In free-electron-like approximation, A_{ee}^S should obey $A_{ee}^S \propto k_F^{-5/2}\ell^{-3/2}$.) Figures 4(a) and 4(b) show A_{ee}^S variation with $k_F^{-5/2}\ell^{-3/2}$ and A_{ee}^L as a function of E_F^{-1} , respectively. Here the values of E_F , k_F and ℓ are also determined from the free-electron-like model. As expected, the $A_{ee}^L \propto E_F^{-1}$ and $A_{ee}^S \propto k_F^{-5/2}\ell^{-3/2}$ rules are observed in Fig. 4. According to Eq. (1), the slopes of $A_{ee}^S k_F^{-5/2}\ell^{-3/2}$ and $A_{ee}^L E_F^{-1}$ curves should be $3.41 \times 10^{27} \text{ m}^{-1} \text{ K}^{-3/2} \text{ s}^{-1}$ and $7.10 \times 10^{-13} \text{ J K}^{-2} \text{ s}^{-1}$, respectively. The least-squares fits results indicate the slopes being $9.62 \times 10^{26} \text{ m}^{-1} \text{ K}^{-3/2} \text{ s}^{-1}$ and $5.84 \times 10^{-13} \text{ J K}^{-2} \text{ s}^{-1}$, respectively. The experimental value of the slope of $A_{ee}^L E_F^{-1}$

curve is $\sim 18\%$ smaller than the theoretical one. The consistency between the two values is extremely good. While the experimental and theoretical values of the slope of $A_{ee}^S k_F^{-5/2}\ell^{-3/2}$ curve agree to within a factor of ~ 3 . This level of agreement is also satisfactory.

As mentioned above, the carrier concentrations of the In_2O_3 films are $\sim 5 \times 10^{19} \text{ cm}^{-3}$, which are 3-4 orders of magnitude lower than that in typical metals. Hence the e -ph relaxation rates of the In_2O_3 films are greatly suppressed and the e - e scattering rates are much enhanced. The $k_F\ell$ value of the In_2O_3 film is about twice as large as that in ITO films used in Ref. 14, while the carrier concentration of the former is about one fourth of that of the latter. Since the Fermi energy $E_F \propto n^{2/3}$, the small-energy-transfer e - e scattering strength A_{ee}^S of the In_2O_3 film would be much less than that of the ITO film used in Ref. 14, while the large-energy-transfer e - e scattering strength A_{ee}^L in the former would be great than that in the latter (see Eq. (1)). That is why the electron dephasing process in ITO films is only governed by the small-energy-transfer e - e scattering and both the large- and small-energy-transfer e - e scattering process have to be considered in In_2O_3 films. In a word, these characteristics of relative large $k_F\ell$ and low carrier concentrations of In_2O_3 thick films give us opportunity to simultaneously observe small- and large-energy-transfer electron-electron scattering in 3D disordered conductors, and for the first time fully demonstrate the 3D e - e scattering rate deduced 40 years ago.

IV. CONCLUSION

We have studied the temperature behavior of resistivity and the electron dephasing rate in low temperature regime in In_2O_3 thick films. The $\rho(T)$ data obey Bloch-Grüneisen law from 300 down to ~ 100 K, indicating the films possess degenerate semiconductor characteristic in electrical transport properties. The e -ph scattering rate is negligibly weak though the In_2O_3 films are 3D with regard to WL effect. On the contrary, the e - e inelastic scattering govern the low temperature dephasing processes. In addition, besides the small-energy-transfer e - e scattering, the large-energy-transfer e - e scattering also has significant contribution to the total electron relaxation rate. Our results also quantitatively demonstrate the validity of the theoretical predications of both small- and large-energy-transfer e - e scattering rates in experiment.

ACKNOWLEDGMENTS

This work was supported by the National Natural Science Foundation of China (NSFC) through Grant No. 11174216, Research Fund for the Doctoral Program of Higher Education through Grant No. 20120032110065.

-
- * Author to whom correspondence should be addressed.
Electronic mail: zhiqingli@tju.edu.cn
- ¹ A. Schmid, Z. Phys. **271**, 251 (1974).
 - ² B. L. Altshuler and A. G. Aronov, JETP Lett. **30**, 482 (1979).
 - ³ B. L. Altshuler and A. G. Aronov, in *Electron-Electron Interactions in Disordered Systems*, edited by A. L. Efros and M. Pollak (Elsevier, Amsterdam, 1985).
 - ⁴ Z. Ovadyahu, Phys. Rev. Lett. **52**, 569 (1984).
 - ⁵ A. Stolovits, A. Sherman, K. Ahn and R. K. Kremer, Phys. Rev. B **62**, 10565 (2000).
 - ⁶ T. Andrearczyk, J. Jaroszyński, G. Grabecki, T. Dietl, T. Fukumura and M. Kawasaki, Phys. Rev. B **72**, 121309R (2007).
 - ⁷ T. Dietl, T. Andrearczyk, A. Lipińska, M. Kiecana, M. Tay and Y. Wu, Phys. Rev. B **76**, 155312 (2000).
 - ⁸ X. D. Liu, E. Y. Jiang, and D. X. Zhang, J. Appl. Phys. **104**, 073711 (2008).
 - ⁹ J. J. Lin and J. P. Bird, J. Phys.: Condens. Matter **14**, R501 (2002).
 - ¹⁰ J. Rammer and A. Schmid, Phys. Rev. B **34**, 1352 (1986).
 - ¹¹ Y. L. Zhong and J. J. Lin, Phys. Rev. Lett. **80**, 588 (1998).
 - ¹² Z. Q. Li and J. J. Lin, J. Appl. Phys. **96**, 5918 (2004).
 - ¹³ J. J. Lin and Z. Q. Li, J. Phys.: Condens. Matter **26**, 343201 (2014).
 - ¹⁴ Y. J. Zhang, Z. Q. Li, and J. J. Lin, Europhys. Lett. **103**, 47002 (2013).
 - ¹⁵ Y. J. Zhang, Z. Q. Li and J. J. Lin, Phys. Rev. B **84**, 052202 (2011).
 - ¹⁶ J. M. Ziman, *Electron and Phonons* (Clarendon Press, Oxford, 1960), p. 364.
 - ¹⁷ W. J. Lang and Z. Q. Li, Appl. Phys. Lett. **105**, 042110 (2014).
 - ¹⁸ S. P. Chiu, J. G. Lu, and J. J. Lin, Nanotechnology **24**, 245203 (2013).
 - ¹⁹ B. L. Altshuler, D. Khmelnitzkii, A. I. Larkin, and P. A. Lee, Phys. Rev. B **22**, 5142 (1980).
 - ²⁰ P. A. Lee and T. V. Ramakrishnan, Rev. Mod. Phys. **57**, 287 (1985).
 - ²¹ G. Bergmann, Phys. Rep. **107**, 1 (1984).
 - ²² Int. J. Mod. Phys. B **24**, 2015 (2010).
 - ²³ S. Lany and A. Zunger, Phys. Rev. Lett. **98**, 045501 (2007).
 - ²⁴ F. A. Kröger, *The Chemistry of Imperfect Crystals* (North-Holland, Amsterdam, 1974), 2nd ed.
 - ²⁵ J. H. W. de Wit, J. Solid State Chem. **13**, 192 (1975).
 - ²⁶ J. H. W. de Wit, G. van Unen, and M. Lahey, J. Phys. Chem. Solids **38**, 819 (1977).
 - ²⁷ A. Ambrosini, G. B. Palmer, A. Maignan, K. R. Poeppelmeier, M. A. Lane, P. Brazis, C. R. Kannewurf, T. Hogan, and T. O. Mason, Chem. Mater. **14**, 52 (2002).
 - ²⁸ P. Agoston, K. Albe, R. M. Nieminen, and M. J. Puska, Phys. Rev. Lett. **103**, 245503 (2009).
 - ²⁹ S. Lany and A. Zunger, Phys. Rev. Lett. **106**, 069601 (2011).
 - ³⁰ P. Agoston, K. Albe, R. M. Nieminen, and M. J. Puska, Phys. Rev. Lett. **106**, 069602 (2011).
 - ³¹ S. Lany, A. Zakutayev, T. O. Mason, J. F. Wager, K. R. Poeppelmeier, J. D. Perkins, J. J. Berry, D. S. Ginley, and A. Zunger, Phys. Rev. Lett. **108**, 016802 (2012).
 - ³² A. Kawabata, Solid State Commun. **34**, 431 (1980).
 - ³³ A. Kawabata, J. Phys. Soc. Jpn. **49**, 628 (1980).
 - ³⁴ H. Fukuyama and K. Hoshino, J. Phys. Soc. Jpn. **50**, 2131 (1981).
 - ³⁵ C. Y. Wu and J. J. Lin, Phys. Rev. B **50**, 385 (1994).
 - ³⁶ D. V. Baxter, R. Richter, M. L. Trudeau, R. W. Cochrane, and J. O. Strom-Olsen, J. Phys. Paris **50**, 1673 (1989).
 - ³⁷ A. Sergeev and V. Mitin, Phys. Rev. B **61**, 6041 (2000).
 - ³⁸ Y. L. Zhong, A. Sergeev, C. D. Chen, and J. J. Lin, Phys. Rev. Lett. **104**, 206803 (2010).
 - ³⁹ The value of $qT\ell$ is evaluated through $qT\ell \approx k_B T\ell/\hbar u_t$, where u_t is the transverse sound velocity.
 - ⁴⁰ J. J. Lin and N. Giordano, Phys. Rev. B **35**, 1071 (1987).
 - ⁴¹ P. Mohanty, E. M. Q. Jariwala, and R. A. Webb, Phys. Rev. Lett. **78**, 3366 (1997).
 - ⁴² S. M. Huang, T. C. Lee, H. Akimoto, K. Kono, and J. J. Lin, Phys. Rev. Lett. **99**, 046601 (2007).
 - ⁴³ T. Wittkowski, J. Jorzick, H. Seitz, B. Schroder, K. Jung, and B. Hillebrands, Thin Solid Films **465**, 398 (2001).
 - ⁴⁴ I. Hamberg, C. G. Granqvist, K. F. Berggren, B. E. Sernelius, and L. Engström, Phys. Rev. B **30**, 3240 (1984).